IL NUOVO CIMENTO Vol. 35 C, N. 5 Settembre-Ottobre 2012
DOI 10.1393/ncc/i2012-11320-8

Communications: SIF Congress 2011

Rare-earth–activated glass ceramics for use as solar-cell down-converter layers

D. Ristić(*)
CNR-IFN, CMSFO lab - Via alla Cascata 56/C, 38123 Povo (Trento), Italy

ricevuto il 21 Dicembre 2011; revisionato l' 8 Febbraio 2012; approvato l' 11 Marzo 2012

Summary. — The efficiency of a solar cell can be increased by using photon management to make better use of the solar spectrum. In particular the down-conversion process which permits us to obtain two low-energy (980 nm) photons from one high-energy photon. In particular we present a system consisting of a 70 SiO_2-30 HfO_2 glass ceramic waveguide co-doped with Tb^{3+} and Yb^{3+} ions. We present the assesment of the energy transfer efficiency from an excited Tb^{3+} ion to two Yb^{3+} ions in its vicinity.

PACS 88.40.hj – Efficiency and performance of solar cells.

1. – Introduction

The efficiency of a standard silicon solar cell is limited by the fact that only a part of the solar spectrum around and slightly above the energy of the silicon band gap (1.1 eV, around 1100 nm) can be efficiently converted into electricity [1]. Therefore, a major part of the solar spectrum is lost, namely the entire blue and ultraviolet part of the spectrum and the entire infrared part of the spectrum with wavelengths above 1100 nm. To increase the efficiency of the solar cell different photon management schemes can be used including down-shifting, down-conversion or up-conversion [1]. In all these schemes an additional layer is placed on top of the solar cell to convert some of the photons of the incoming solar light into near infrared photons (around 1000 nm) that can be efficiently converted into electrical energy by the solar cell. Rare-earth ions have been extensively employed both for the down-converter and up-converter applications. Rare earths have very sharp energy levels with long lifetimes (in the range of ms) which make high internal energy conversion efficiencies possible. Although single rare-earth ion down-conversion is possible [3], usually two different rare earths are employed to achieve the down-conversion effect. One rare-earth ion used is usually Yb^{3+}, since its emission is at 980 nm which is

(*) E-mail: ristic@fbk.eu

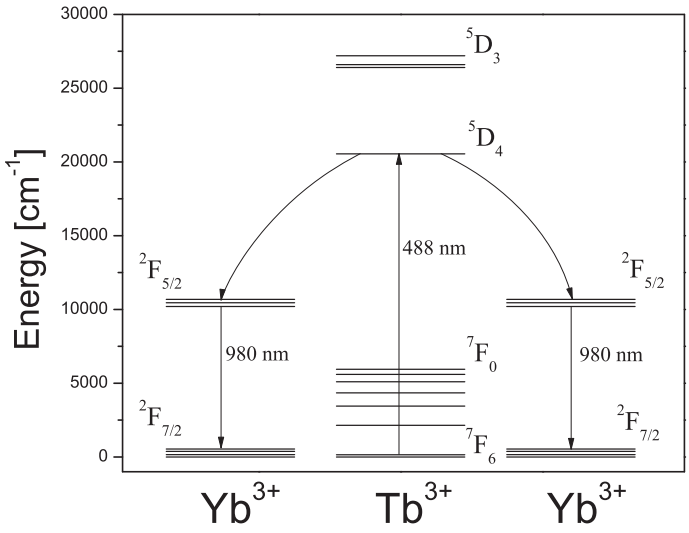

Fig. 1. – Energy diagram of the Tb^{3+}-Yb^{3+} down-converter system.

around the maximum of silicon absorption. However since Yb^{3+} does not absorb in the blue or ultraviolet region, an additional rare earth is used to absorb the solar radiation and transfer the energy to the Yb^{3+} ions. Different rare earths that can be employed are Pr^{3+} [4,5], Eu^{3+} [6], Tb^{3+} [7-10] or Tm^{3+} [11,12]. In particular the Tb^{3+}-Yb^{3+} system was found to be an efficient blue (488 nm) to near-infrared (980 nm) down-converter. This down-conversion mechanism is sketched in fig. 1. The Tb^{3+} ion absorbs a blue photon at 488 nm and is excited in its $^5D_4$ state. Afterwards it de-excites non-radiatively by transferring its energy to two Yb^{3+} ions which are then excited from their ground state to their $^2F_{5/2}$ state. Afterwards the two Yb^{3+} ions de-excite by emitting a 980 nm photon each.

The choice of the matrix is a crucial point to address if an efficient down-conversion mechanism is wanted. The matrix has to be chosen to reduce the non-radiative transitions from the rare-earth ions to the host matrix. Sol-gel–derived glass ceramics have recently been shown to be a good choice for the matrix in quantum cutting processes [13]. In particular, it has been shown that the Er^{3+} ions remain incorporated inside the HfO_2 nanocrystals. This leads to the decrease of the non-radiative de-excitation probability, since the phonon energies in HfO_2 are considerably lower than in the case of silica ($700\,cm^{-1}$ with respect to $1100\,cm^{-1}$). In this paper we will present the down-conversion of a 70 SiO_2-30 HfO_2 glass ceramic waveguide co-doped with Tb^{3+} and Yb^{3+} ions [2].

2. – Experimental set-up

The Tb^{3+} and Yb^{3+} and doped glass ceramics described in this paper were produced in the following manner [2]. The films were produced using the dip coating method from a sol-gel precursor. The starting solution, obtained by mixing tetraethylorthosilicate (TEOS), ethanol, deionized water and hydrochloric acid as a catalyst, was pre-hydrolyzed for 1 hour at 65 °C. The molar ratio of TEOS : HCl : EtOH : H_2O was 1 : 0.01 : 37.9 : 2. An ethanolic colloidal suspension was prepared using as a precursor $HfOCl_2$ and then added to the TEOS solutions, with a Si/Hf molar ratio of 70:30. Terbium and ytterbium

TABLE I. – *Rare-earth concentrations for two sets of samples.*

Sample label	Tb^{3+} (mol%)	Yb^{3+} (mol%)
AR1	0.5	0
A1	0.5	1
A2	0.5	2
A3	0.5	3
BR1	0.2	0
B1	0.2	0.8
BR2	0.6	0
B2	0.6	2.4
BR3	1	0
B3	1	4

were added as $Tb(NO_3)_3 \times 5H_2O$ and $Tb(NO_3)_3 \times 5H_2O$. The molar concentrations of the Tb^{3+} and Yb^3 ions were varied to obtain different samples. The final mixture was left at room temperature under stirring for 16 h. The obtained sol was filtered with a 0.2 μm Millipore filter. Rare-earth–doped silica-hafnia layers were deposited on a cleaned silica slide by dip-coating, with a dipping rate of 40 mm/min. After each dip, the sample was densified in air for 50 s at 900 °C. Every ten dips the samples were made to undergo an additional densification for 2 min at 900 °C and at the end the final sample was densified for 5 min at 900 °C. In this manner glass waveguides were produced. To produce the glass-ceramic waveguides the glass waveguides were made to undergo an additional heat treatment at 1000 °C for 30 min. Table I gives the compositional parameters of the produced samples.

The thickness and refractive index of different samples were determined using an m-line apparatus at 543.5 nm and 632.8 nm and were found to be around $1.0 \pm 0.1\,\mu$m and 1.62 ± 0.02 for all the produced samples. The refractive index was always found to be greater at 543.5 nm than at 632.8 nm by a factor of 0.005. The luminescence measurements were made both in the visible and in the infrared region of the spectrum. The measurements in the infrared were made upon excitation with the 476 nm line of the Ar^+ ion laser. The spectra were made in the region 960–1060 nm corresponding to the $^2F_{5/2} \rightarrow {}^2F_{7/2}$ transition of the Yb^{3+} ions using a single grating monocromator with a resolution of 2 nm and a Si/InGaAs two-color photodiode and standard lock-in technique. In the visible the measurements were made upon excitation with the third harmonic of the Nd-YAG laser at 352 nm. The spectra were recorded using a monocromator with a 5 cm^{-1} resolution and with a photon-counting system. The decay curves were obtained recording the signal with a Stanford SR430 multichannel analyzer.

3. – Results

The first series of samples, labelled A, were made so that the Yb^{3+} concentration was varied and the Tb^{3+} concentration was kept constant. This was done in order to determine the optimum Yb^{3+}-to-Tb^{3+} ratio. Figure 2 shows the luminescence spectra of these samples upon excitation at 476 nm.

The intense emission band centered at 977 nm, with a shoulder at 1027 nm is attributed to the $^2F_{5/2} \rightarrow {}^2F_{7/2}$ transition of the Yb^{3+} ions. The presence of the Yb^{3+}

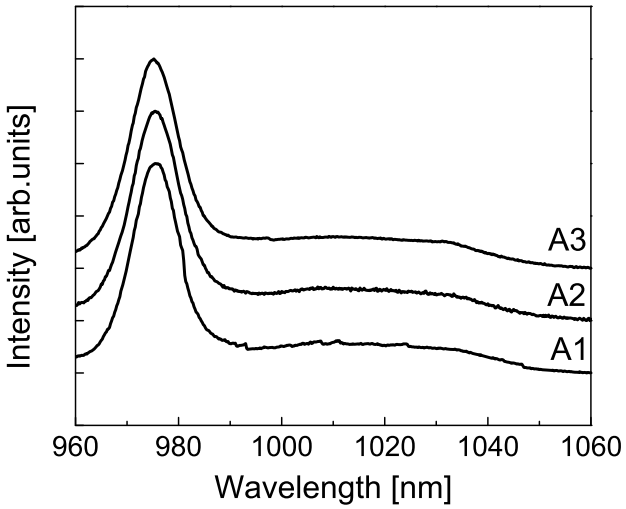

Fig. 2. – Room temperature luminescence spectra of the ${}^2F_{5/2} \rightarrow {}^2F_{7/2}$ transition of the Yb^{3+} ions upon excitation at 476 nm for the samples of the A series.

emission is an indication of the energy transfer between the Tb^{3+} and Yb^{3+} ions and hence of an efficient down-conversion. To measure the efficiency of this energy transfer the decay measurement of the ${}^5D_4$ energy level of the Tb^{3+} ion has to be made. This decay can be measured by monitoring the ${}^5D_4 \rightarrow {}^7F_5$ transition at 543 nm. The luminescence of one of the samples measured in the spectral region around 543 nm is presented in fig. 3. The vertical line indicates the position of the ${}^5F_4 \rightarrow {}^7F_{5/2}$ transition used in the decay measurements.

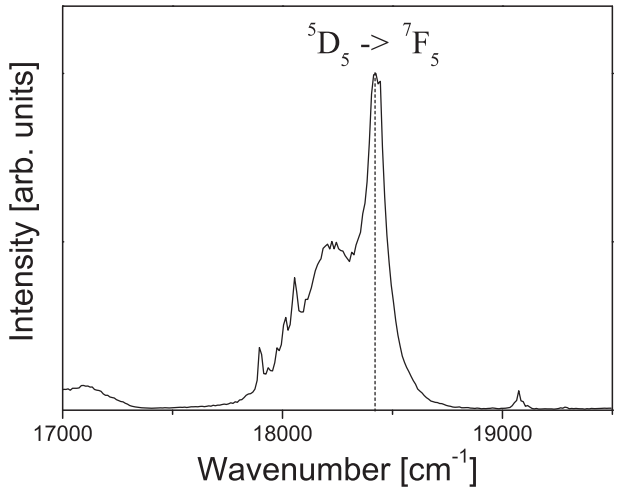

Fig. 3. – The luminescence spectra of a Tb^{3+}, Yb^{3+} co-doped sample showing the ${}^5D_4 \rightarrow {}^7F_5$ transition of the Tb^{3+} ion. The vertical line shows the wavelength at which all subsequent decay measurements were made.

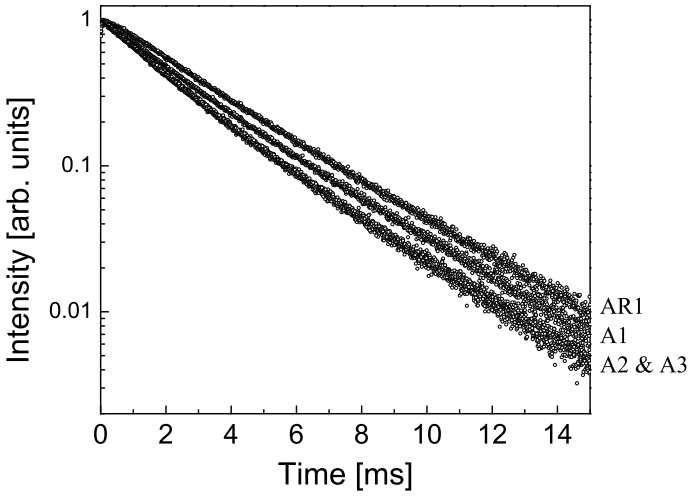

Fig. 4. – Decay measurements of the $^5D_4$ metastable state of the Tb^{3+} ion measured by monitoring the $^5D_4 \rightarrow {}^7F_5$ transition at 543 nm for the A series of samples. The decays of the samples A2 and A3 are overlapping and cannot be distinguished one from the other.

If we define the energy transfer efficiency as the number of Tb^{3+} ions excited in their $^5D_4$ state that will de-excite non-radiatively by transferring their energy to a pair of Yb^{3+} ions in their vicinity, it can be shown [10] that this energy transfer efficiency can be calculated by considering the ratio of the integrated intensity of the decay curves of the Tb^{3+}-Yb^{3+} co-doped sample and the Tb^{3+} single-doped sample:

$$\eta_{\text{Tb-Yb}} = \frac{\int I_{\text{Tb-Yb}} \mathrm{d}t}{\int I_{\text{Tb}} \mathrm{d}t}\,. \tag{1}$$

In some papers a quantity called the effective quantum efficiency defined as the ratio of the number of absorbed photons to the number of emitted photons is used. The effective quantum efficiency is linearly proportional to the above-defined energy transfer efficiency if we set quantum efficiency of the Tb^{3+} ions to unity [10]:

$$\eta_{\text{EQE}} = 1 + \eta_{\text{Tb-Yb}}. \tag{2}$$

In fig. 4 the decay curves of the $^5F_4 \rightarrow {}^7F_{5/2}$ transition measured at 543 nm upon excitation at 355 nm are given. A decrease of the lifetime with the increase of the Yb^{3+} content is observed, indicating an increase of the energy transfer efficiency with the increase of Yb^{3+} content. In table II the energy transfer efficiencies and effective quantum efficiencies calculated according to eqs. (1) and (2) are given for the glass ceramic samples of the A series. The results presented in table II show that the transfer efficiency increases with increasing the Yb^{3+}/Tb^{3+} ratio. However, when increasing the density of active ions concentration quenching can become important too. This seems to be the reason why the energy transfer efficiency does not exceed 25% for the A series of samples.

In table II the efficiencies for the samples with the same rare-earth content but in a glassy matrix are also given. As expected, the estimated quantum efficiencies are greatly

TABLE II. – *Transfer efficiencies for the A series of samples.*

Sample label	Energy transfer efficiency	Effective quantum efficiency
Glass-ceramic		
A1	14%	114%
A2	24%	124%
A3	25%	125%
Glass		
A1	2%	102%
A2	4%	104%
A3	6%	106%

reduced in the glassy matrix with respect to the glass ceramic case. It seems that the reduction of non-radiative relaxation channels due to the low cut-off frequency of the HfO_2 nanocrystals plays a key role in the energy transfer efficiency between Tb^{3+} and Yb^{3+} ions.

In the second series of samples, labelled B, the Yb^{3+}/Tb^{3+} ratio was kept constant at $Yb^{3+}/Tb^{3+} = 4$ while the overall rare-earth content in the glass-ceramic was increased from 1 to 5 mol%. In fig. 5 the Yb^{3+} emission is presented for the samples of the B series. Similarly as for the A series, the Yb^{3+} emission at 980 nm indicates that there is energy transfer between Tb^{3+} and Yb^{3+} ions.

To determine the energy transfer efficiencies the same type of analysis was done as for the A series of samples. The decay curves of the samples of the B series and the

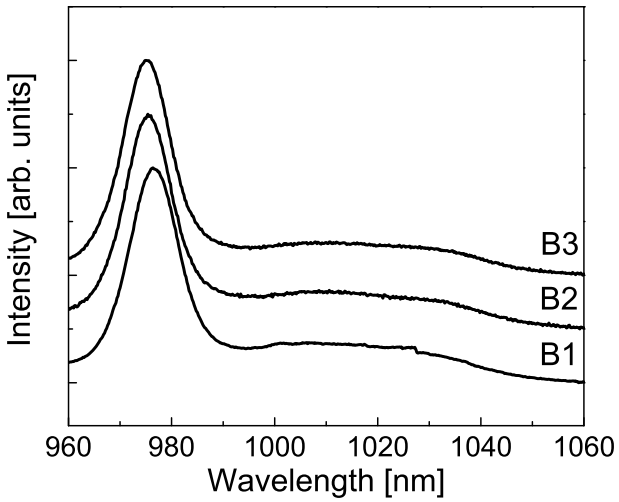

Fig. 5. – Room temperature luminescence spectra of the ${}^2F_{5/2} \rightarrow {}^2F_{7/2}$ transition of the Yb^{3+} ions upon excitation at 476 nm for the samples of the B series.

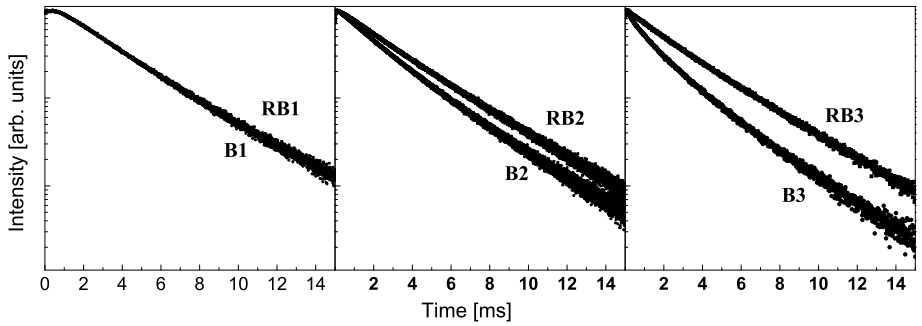

Fig. 6. – Decay measurements of the $^5D_4$ metastable state of the Tb^{3+} ion measured by monitoring the $^5D_4 \rightarrow {}^7F_5$ transition at 543 nm for the B series of samples.

TABLE III. – *Transfer efficiencies for the B series of samples.*

Sample label	Energy transfer efficiency	Effective quantum efficiency
Glass-ceramic		
B1	1%	101%
B2	18%	118%
B3	38%	138%

corresponding transfer efficiencies are presented in fig. 6 and table III. The increase of the energy transfer efficiency with the increase of the overall rare-earth content in the samples is evident, the highest energy transfer efficiency obtained being 38% for the sample with 5 mol% of the overall rare-earth content.

4. – Conclusion

In summary, efficient Tb^{3+}-Yb^{3+} co-doped 70 SiO_2-30 HfO_2 glass ceramics were produced for use as down-converter layers. Near-infrared emission at 980 nm assigned to the $^2F_{5/2} \rightarrow {}^2F_{7/2}$ transition of the Yb^{3+} ions was observed upon excitation at 476 nm. The energy transfer efficiencies were estimated from the decay curves of the $^5D_4$ metastable state of the Tb^{3+} ion. The highest energy transfer efficiency was found to be 38% for the sample doped with 1 mol% of Tb^{3+} and 4 mol% Yb^{3+}.

* * *

I am strongly indebted with my colleagues G. ALOMBERT GOGET (Université de Versailles), B. DIEUDONNE and B. BOULARD (LdOF, Université du Maine), E. MOSER (University of Trento), S. BERNESCHI, S. PELLI (IFAC-CNR Firenze), S. VARAS and M. FERRARI (IFN-CNR Trento). The present activity would not have been possible without their invaluable scientific and technical contribution. This work was done in the framework of the research projects EU cost Action MP0702 and of the NSBMO (2010-2013) project of the Provincia Autonoma di Trento.

REFERENCES

[1] Richards B. S., *Sol. Energy Mater Sol. Cells*, **90** (2006) 1189.
[2] Alombert-Goget G., Armellini C., Berneschi S., Chiappini A., Chiasera A., Ferrari M., Guddala S., Moser E., Pelli S., Rao D. N. and Righini G. C., *Opt. Mater.*, **33** (2010) 227.
[3] Kumar A., Rai D. K. and Rai S. B., *Solid State Commun.*, **117** (2001) 387.
[4] Srivastava A. M., Doughty D. A. and Beers W. W., *J. Electrochem. Soc.*, **143** (1996) 4113.
[5] Chen D., Wang Y., Yu Y., Huang P. and Weng F., *Appl. Phys. B*, **96** (2009) 51.
[6] Wegh R. T., Donker H., Oskam K. D. and Meijerink A., *Science*, **283** (1999) 663.
[7] Strek W., Bednarkiewicz A. and Deren P., *J. Lumin.*, **92** (2001) 229.
[8] Chen J. X., Ye S., Wang X. and Qiu J. R., *Chin. Phys. Lett.*, **25** (2008) 2078.
[9] Liu X., Ye S., Qiao Y., Dong G., Zhu B., Chen D., Lakshminarayana G. and Qiu J., *Appl. Phys. B*, **96** (2009) 51.
[10] Vergeer P., Vlugt T. J. H., Kox M. H. F., Den Hertog M. I., van der Eerden J. P. M. J. and Meijerink A., *Phys. Rev. B*, **71** (2005) 014119.
[11] Ye S., Zhu B., Luo J., Chen J., Lakshminarayana G. and Qiu J., *Opt. Lett.*, **16** (2008) 8989.
[12] Lakshminarayana G., Yang H., Ye S., Liu Y. and Qiu J., *J. Phys. D: Appl. Phys.*, **41** (2008) 175111.
[13] Gonçalves R. R., Carturan G., Zampedri L., Ferrari M., Montagna M., Righini G. C., Pelli S., Ribeiro S. J. L. and Messaddeq Y., *Opt. Mater.*, **25** (2004) 131.